J Inorg Organomet Polym (2015) 25:796–803
DOI 10.1007/s10904-014-0162-5

# Synthesis and Characterization of Perovskite Oxides $LaAl_{1-x}Ni_xO_{3-\delta}$ ($0 \leq x \leq 0.6$) via Co-precipitation Method

**Lynda Djoudi · Mahmoud Omari**

Received: 26 October 2014 / Accepted: 31 December 2014 / Published online: 6 January 2015


**Abstract** Our contribution has focused on the synthesis and characterization of nickel-containing $LaAlO_3$ perovskite, $LaAl_{1-x}Ni_xO_{3-\delta}$ ($0 \leq x \leq 0.6$) by a co-precipitation method. Nano-powders were successfully synthesized using nitrate salts of lanthanum, aluminium and nickel as cations precursors and sodium hydroxide such as base precipitant by this method and calcined at low temperatures. They were characterized by several techniques: Fourier transform infrared spectroscopy, thermogravimetric and differential thermal analysis (TGA/DTA), X-ray diffraction (XRD), scanning electron microscopy and electrochemical measurements. Thermal analysis shows that the crystallization temperature of the La (Al, Ni) $O_{3-\delta}$ precursor gels are estimated as 780 °C by TG–DTA. The XRD patterns of the precursor gels calcined at 700 °C for 6 h have a perovskite structure and the presence of crystalline impurities is not found. The microstructure and morphology of the compounds show that the particles are nearly spherical in shape and are partially agglomerated. Electrochemical measurements indicate that the catalytic activity is strongly influenced by lanthanum doping. The highest electrode performance is achieved with large nickel content.

**Keywords** Perovskite oxide · Coprecipitation · Powder diffraction · Thermal analysis · Electrochemical properties

L. Djoudi · M. Omari (✉)
Laboratory of Molecular Chemistry and Environment, University of Biskra, B. P. 145, 07000 Biskra, Algeria
e-mail: m2omari@yahoo.fr

## 1 Introduction

To search for a new electrolyte with higher ionic conductivity and better stability perovskite-type oxides ($ABO_3$) have received much attention because this unique crystal structure is very tolerant of various sizes of cations at both A- and B-cation sublattices. Thus, aliovalent cations can be dissolved in both A- and B-site cation sublattices. Consequently, oxygen vacancies are generated to compensate the charge of substituting ions. Several oxides with perovskite structures have been studied. Among them, $LaGaO_3$ based oxides [1–7] have been extensively investigated for use as the electrolyte materials for intermediate-temperature (<800 °C) SOFCs.

However, the high cost of gallium compounds and their low mechanical strength are the main obstacles for using $LaGaO_3$ based solid electrolytes in SOFC applications. Therefore, the replacement of Ga with inexpensive element, such as Al, is highly desirable. It was found that rare-earth aluminates exhibit ionic conduction. The conductivity of $LaAlO_3$ was significantly affected by the addition of aliovalent cations [8–19]. The possibility of using aluminate-based materials as electrolytes for SOFC has also been suggested by Iwahara and co-workers [17]. Regardless of the intrinsic properties and the final use of a given perovskite composition, the synthesis of a powder with well defined physical characteristics is the first important step in its successful application.

In recent years, extensive investigations have been performed for preparing finer and more homogeneous powders of pure and substituted $LaAlO_3$ at lower temperatures using various chemical processes. The series of $La_{1-x}M_xAlO_3$ (M = Na, K, Ca, Ba, $x = 0.1$) and $LaAl_{1-x}M_xO_3$ (M = Li, Mg, $x = 0.1$) perovskite-type catalysts were prepared from citrate precursors [20] and calcined at 800 °C for 5 h.

Spinicci et al. [21] have reported that $La_{1-x}M_xAlO_3$ (M = Ca, Ba) oxides exhibited a rhombohedral perovskite structure. Furthermore Ciambelli et al. [22] have obtained pure $LaAl_{1-x}Fe_xO_3$ ($0 \leq x \leq 1$) powders by calcining the precursors at 800 °C for 5 h, via citrate method [20].

Moreover the formation of the solid solutions of $LaAl_{1-x}Mn_xO_3$ ($x = 0.0$–$1.0$) using the citrate method have been studied by Cimino et al. [23]. Recently, a sol–gel method was proposed to produce pure $LaAl_{1-x}Ni_xO_{3-\delta}$ powders [24, 25], by calcining the precursors at 750 °C for 4 h, using the propionic acid as the solvent, with $x$ values varying from 0 to 1 with 0.2 intervals following the method developed in [26]; the critical point of this method is the decomposition of nitrate anions with violent $NO_2$ production which is especially observed in large scale preparations during the evaporation of the solvent. At this regards, this method is even more dangerous than the original route based on citrate because of the presence of propionic acid instead of water.

Unfortunately, all these methods are either complex or expensive, which limited their large scale applications. Chemical coprecipitation route is a simple method for synthesizing nanopowders [27].

In the present study, the goal of this work is to use, an efficient process for perovskite powder production through low calcination temperature but yielding high purity of perovskite phase. Nickel containing $LaAlO_3$ perovskite of the general formula $LaAl_{1-x}Ni_xO_{3-\delta}$, $x$ values varying from 0 to 0.6 with a 0.1 step have been successfully synthesized by coprecipitation route from metal nitrate salt as cations precursors and mixture of sodium hydroxide such as base precipitant at 700 °C for 6 h. The preparation technique, thermal behavior, crystal structure, crystallite size, electrochemical properties, behavior of the low-temperature synthesized $LaAl_{1-x}Ni_xO_{3-\delta}$ nanopowders have been investigated in detail.

## 2 Experimental Procedure

### 2.1 Synthesis of Perovskite-Type Oxides

A series of the perovskite-type $LaAl_{1-x}Ni_xO_{3-\delta}$ compounds with $x = 0$–$0.6$ were synthesized by the co-precipitation method. Aqueous solutions of $La(NO_3)_3 \cdot 6H_2O$, $Al(NO_3)_3 \cdot 6H_2O$ and $Ni(NO_3)_2 \cdot 6H_2O$ with the desired Al/Ni ratio were mixed and precipitated with NaOH. In all cases, after the reaction was completed, the precipitates were washed with distilled water and ethanol for several times, dried overnight at 110 °C to obtain the dry precursors by evaporating the solvent, then the precursors obtained were ground into powders and heat-treated from 700 °C in air for 6 h, at a heating rate of 5°C/min.

### 2.2 Characterization Techniques

The thermal decomposition processes of the precursor gels were studied in air atmosphere by thermogravimetric and differential thermal analyses TG/DTA using a LINSEIS STA PT1600 at a heating rate of 10 °C/min in air. The Fourier transform infrared (FT-IR) absorption spectra were recorded using FT-IR SHIMADZU 8400S spectrometer. X-ray diffraction (XRD) patterns were carried out with a D8 ADVANCE-BRUCKER using a Cu $K_\alpha$ radiation ($\lambda_{K\alpha} = 1.54056$ Å) and a Ni filter. The powder samples were mounted on a flat XRD plate and scanned at room temperature in the range 10°–90° to identify the crystalline phases present in the calcined powders by comparison with Joint Committee on Powder Diffraction Standards (JCPDS) files. Scanning electron microscopy (SEM) was used to examine the particle morphology of the perovskite using a JEOL scanning electron microscope (Model JSM6390LV).

The electrochemical experiments for $O_2$ reduction and evolution were performed using a Volta Lab 40 potentiostat/galvanostat. The measurements were carried out in a three-compartment cell. Potassium hydroxide electrolyte solution (1 M) was prepared by dissolving the required amount of KOH (Merck) into bidistilled water. The working electrodes (1 $cm^2$) were obtained by painting; with an oxide suspension. The counter electrode used was a Pt plate. The reference electrode was Hg/HgO/1 M KOH. All potentials in the text have been referred to this reference electrode.

## 3 Results and Discussion

### 3.1 Thermal Behavior and Phase Formation of the $LaAl_{0.8}Ni_{0.2}O_{3-\delta}$ Precursor

Figure 1, illustrates the TG/DTA curves of the $LaAl_{0.8}Ni_{0.2}O_{3-\delta}$ precursor heated at a rate of 10 °C/min in the

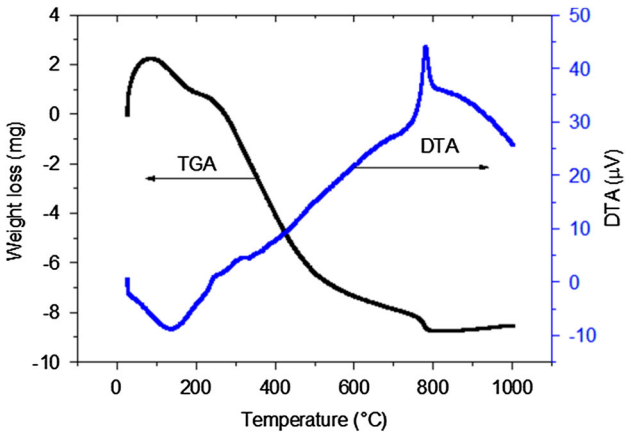


**Fig. 1** DTA/TG curves of the $LaAl_{0.8}Ni_{0.2}O_{3-\delta}$ precursor powders with a heating rate of 10 °C/min

temperature range between 25 and 1,000 °C in static air. The TG curve shows the first weight loss below 140 °C (−9.09 %) corresponds to adsorbed and chemisorbed water. The second weight loss between 140 and 320 °C (−20.45 %) can be ascribed to the decomposition and burnout of most sodium nitrate in the precursor powder, in agreement with previous reports [28, 29]. The third weight loss (−50 %) between 320 and 520 °C is mostly due to the formation of oxides of La, Al and Ni by dehydration of the lanthanum, aluminium and nickel hydroxides, this result agrees with results reported by others authors [29–33]. The weight loss (−15.91 %) between 520 and 760 °C with a clear plateau is may be attributed to the rearrangement of these oxides to the perovskite $LaAl_{0.8}Ni_{0.2}O_{3-\delta}$, in accordance with the XRD results (Fig. 7). The final weight loss (−4.54 %) between 760 and 780 °C is probably due to the removal of residual nitrates, as confirmed by FT-IR analysis (Fig. 3). The thermal decomposition behaviour is associated with endothermic and exothermic effects in the DTA curve shows in Fig. 1 also reveals that the first decomposition step assignable to removal of adsorbed and chemisorbed water is indicated by a broad endothermic peak below 140 °C. One weak exothermic peak at about 320 °C is attributed to the decomposition of lanthanum aluminium and nickel hydroxides. The sharp exothermic peak at 780 °C is due to the formation of the $LaAl_{0.8}Ni_{0.2}O_{3-\delta}$ crystallization. This latter sharp exothermic peak attributable to the formation of the oxide was also found for $LaAlO_3$ synthesized through the coprecipitation route [34, 35].

### 3.2 Infrared Spectra

IR analysis of synthesized samples is important both for the control of the reaction process and the properties of materials obtained. The infrared spectra of the $LaAl_{1-x}Ni_xO_{3-\delta}$ samples (Fig. 2) are presented in the 700–4,000 $cm^{-1}$ region of the IR spectrum. Two strong absorption bands were observed around 670 and 447 $cm^{-1}$. The higher frequency band around 670 $cm^{-1}$ was assigned to the M–O stretching vibration mode (possible La–O, Al–O or Ni–O stretching frequencies vibrations), which involves the internal motion of a change in M–O bond length and the lower frequency band around 447 $cm^{-1}$ corresponds to the bending mode which is sensitive to a change in the M–O–M bond angle (M = Al or Ni). These two bands are related to the environment surrounding the $MO_6$ octahedral in the $ABO_3$ perovskite [36].

No specific peaks of inorganic residues were observed suggesting the high purity of the resulting powders. These results are in accordance with the XRD analysis (Fig. 4) which confirmed the formation of only crystalline phase in $LaAl_{1-x}Ni_xO_{3-\delta}$ nanopowders. The FT-IR spectra for $x = 0$–0.6 show similar patterns. Moreover, it should be

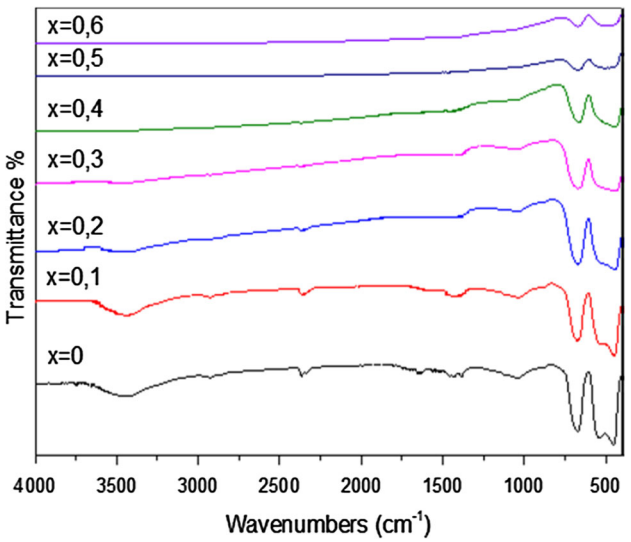


**Fig. 2** FT-IR absorption spectra of the $LaAl_{1-x}Ni_xO_{3-\delta}$ perovskites ($0 \leq x \leq 0.6$) samples calcined at 700 °C

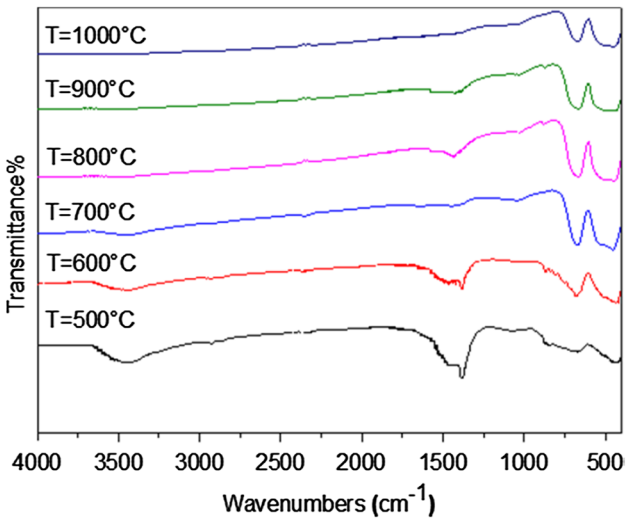


**Fig. 3** Infrared spectra of the $LaAl_{0.8}Ni_{0.2}O_{3-\delta}$ powder sample calcined at different temperatures

observed that the bands related to metal oxygen bonds at 447–420, 670–643 $cm^{-1}$ broaden when nickel is added to the perovskite in accordance with the XRD results (Fig. 5). This supposed to be a result of two different crystallographic positions of B cations existing in the rhombohedrally-distorted perovskite lattice. Similar tendency have been found previously for samples with $La_{1-x}Ca_xCoO_3$ [37], $LaCo_xFe_{1-x}O_3$ and $LaNi_xFe_{1-x}O_3$ oxides [38].

Figure 3, shows the infrared spectra of the $LaAl_{0.8}Ni_{0.2}O_{3-\delta}$ precursor powders, heated at various temperatures for 6 h. A broad absorption in the spectrum of the precursor powder at around 3,400 $cm^{-1}$ at 500–700 °C are probably related to the stretching vibration of the free

hydroxyl group which indicates also the presence of adsorbed water [39]. However, the relatively strong bands at 1,480–1,390 $cm^{-1}$ are due to the stretch vibrations in $NO_3^-$ [40, 41]. These bands disappear with increasing temperature, suggesting the decomposition of the residual material of the synthesis process. These results are in agreement with the TG/DTG curves. In the 700–400 $cm^{-1}$ region of the IR spectrum, two specific observed bands at about 670 and 447 $cm^{-1}$ may be attributed to the characteristic M–O vibrations [42, 43]. At T > 700 °C, they are the only distinguishable transmittance bands detected in the specimen [36, 43] in accordance with the XRD results (Fig. 7) which confirmed the formation of only crystalline phase in $LaAl_{0.8}Ni_{0.2}O_{3-\delta}$ nanopowders.

### 3.3 Phase Characterization of the $LaAl_{1-x}Ni_xO_{3-\delta}$ Catalysts Powders

The XRD patterns of the catalysts powders $LaAl_{1-x}Ni_xO_{3-\delta}$ ($0 \leq x \leq 0.6$) obtained by co-precipitation route after calcination at 700 °C for 6 h summarized in Fig. 4, were compared to the relevant data in the Data Bank available in the diffractometer. The results reveal that all $LaAl_{1-x}Ni_xO_{3-\delta}$ samples are perovskite-type structure with no detectable secondary phase; therefore, all the main diffraction peaks could be indexed in the rhombohedral system. They are in excellent accord with JCPDS card 31-0022. This result indicates that the perovskite structure is well maintained after substitution.

Moreover, powders prepared by the co-precipitation method with $x$ values varying from 0 to 0.6 with 0.1 intervals exhibited similar structure compared to the same powders prepared by the sol–gel methodology [24, 25]. The $LaAl_{1-x}Ni_xO_{3-\delta}$ samples show the same X-ray pattern of $LaAlO_3$. However, the structure peaks shift regularly with increasing $x$ values. An enlargement of the area in the XRD diagram for $2\theta$ between 33.1° and 33.5° shows this progressive shift for the most intensive diffraction peak (110) of $LaAl_{1-x}Ni_xO_{3-\delta}$ structures (Fig. 5).

The lattice parameters of the perovskites $LaAl_{1-x}Ni_xO_{3-\delta}$ were calculated for each $x$ value from the XRD patterns using Celref programme. The values of $a$ and $c$ cell parameters (Å) versus the degree of substitution $x$ are summarized in Table 1. We observe that both parameters increase with increasing Ni content in the samples, this feature is explained considering that smaller $Al^{3+}$ ions are substituted by bigger Ni species in the octahedral sites of the perovskite frame work (ionic radius of $Al^{3+}$ (CN: XI) and $Ni^{2+}$ (CN: XI) are equal to 0.54 and 0.72 Å (Low-spin) respectively [43]. The observed linear expansion of the unit cell volume V with $x$ is shown in Fig. 6. It follows Vegard's law that defines solid solutions, that is to say, they show a linear variation with respect to the substitution degree, confirming the solid solution formation. A similar observation was found in $LaAl_{1-x}Fe_xO_3$ and $LaNi_{1-x}Co_xO_3$ systems ($0 \leq x \leq 1$) [22, 44].

Figure 7, illustrates the XRD patterns of the $LaAl_{0.8}Ni_{0.2}O_{3-\delta}$ powders calcined at different temperatures for 6 h. The XRD patterns of the $LaAl_{0.8}Ni_{0.2}O_{3-\delta}$ powders calcined at 500 and 600 °C for 6 h reveal that the crystalline phase is the rhombohedral with poor crystallinity, the $La_2O_3$ (JCPDS 01-074-2430) phase is detected and no reflections from $Al_2O_3$ and NiO are observed as distinct intermediate phases to the formation of $LaAl_{0.8}Ni_{0.2}O_{3-\delta}$ during the thermal decomposition of the precursor powders even at 1,000 °C. The precursor powders calcined at 700–1,000 °C show good crystallinity of the rhombohedral structure of $LaAl_{0.8}Ni_{0.2}O_{3-\delta}$. These XRD peaks confirm

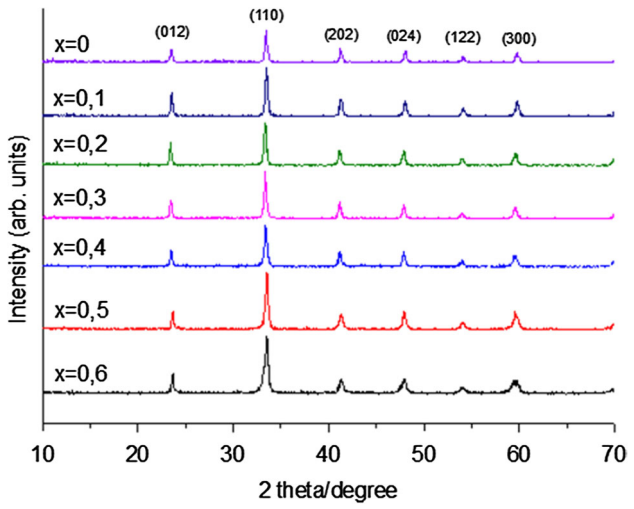


**Fig. 4** X-ray diffraction patterns of perovskite samples $LaAl_{1-x}Ni_xO_{3-\delta}$ ($0 \leq x \leq 0.6$)

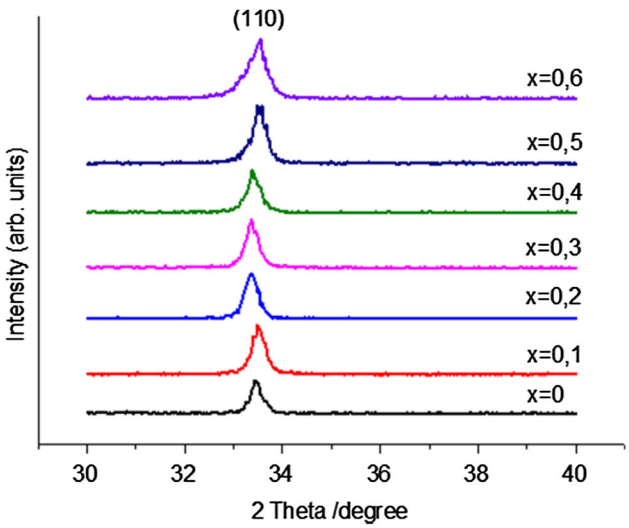


**Fig. 5** Evolution of the position of the highest X-ray diffraction peak

**Table 1** Lattice parameters for $LaAl_{1-x}Ni_xO_{3-\delta}$

| Ni content $x$ | a = b (Å) | c (Å) | V $(Å)^3$ |
|---|---|---|---|
| 0 | 5.3640 | 13.1100 | 326.671 |
| 0.1 | 5.3685 | 13.1171 | 326.885 |
| 0.2 | 5.3695 | 13.1183 | 327.569 |
| 0.3 | 5.3739 | 13.1193 | 327.856 |
| 0.4 | 5.3764 | 13.1199 | 328.186 |
| 0.5 | 5.3806 | 13.1640 | 329.301 |
| 0.6 | 5.3817 | 13.2029 | 330.180 |

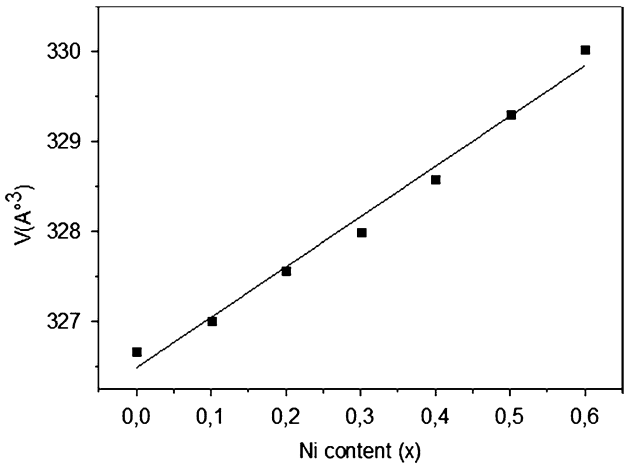


**Fig. 6** Lattice volume dependence on nickel content ($x$) for $LaAl_{1-x}Ni_xO_{3-\delta}$

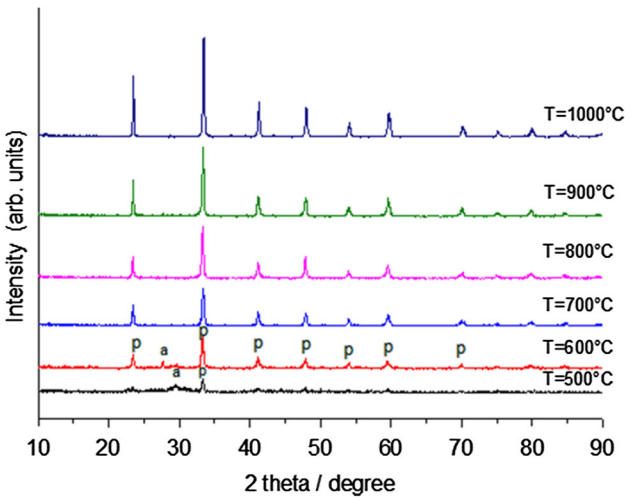


**Fig. 7** XRD patterns of the $LaAl_{0.8}Ni_{0.2}O_{3-\delta}$ powder calcined at different temperatures: (*a*) $La_2O_3$; (*p*) rhombohedral phase

that all samples maintain the perovskite-like structure as all they were identified with the JCPDS file 31 0022. Moreover, these results reconfirm also that the exothermic peak of Fig. 1 at 780 °C is due to the formation of the $LaAl_{0.8}Ni_{0.2}O_{3-\delta}$ perovskite oxide.

The difference in the crystallization temperature of $LaAl_{0.8}Ni_{0.2}O_{3-\delta}$ as observed in DTA and XRD could be caused to the difference in heating schedule from the two samples. While XRD Pattern was recorded on samples which were held for 6 h at 700 °C, the DTA was done without any isothermal hold. Thus the isothermal hold at 700 °C has accelerated the transformation to $LaAl_{0.8}Ni_{0.2}O_{3-\delta}$ at lower temperature. A similar situation has been reported also for $LaAlO_3$ prepared by EDTA, co-precipitation routes and $LaCoO_3$ prepared by mechanochemical activation method [31, 35, 45–47]. With increasing heating, the diffraction peaks become stronger and sharper reflecting greater crystallization.

### 3.4 Structural and Morphological Characterization

The average crystallite size (D) was evaluated from the broadening of the XRD line width by applying the Scherer's formula (Fig. 8). It is observed that crystallite size decreases with increasing nickel content. This is probably due to the incorporation of $Ni^{2+}$ into the $LaAlO_3$ lattice which leads to the crystallite decrease. Similar tendency has been found previously for $La_{1-x}Sr_xMnO_3$ samples synthesized by coprecipitation of precursor acetates [48] and $LaCo_{1-x}Ru_xO_3$ [49] prepared by Pechini sol–gel method.

The SEM micrographs of the $LaAl_{1-x}Ni_xO_{3-\delta}$ compounds are shown in Fig. 9. The micrographs indicate clearly that the shape remains similar which the samples particles are nearly spherical in shape and the powders are partially agglomerated. The average grain sizes of the powders are approximately 0.14–0.27 μm. The formation of agglomerate is probably due to the nature of the solvent

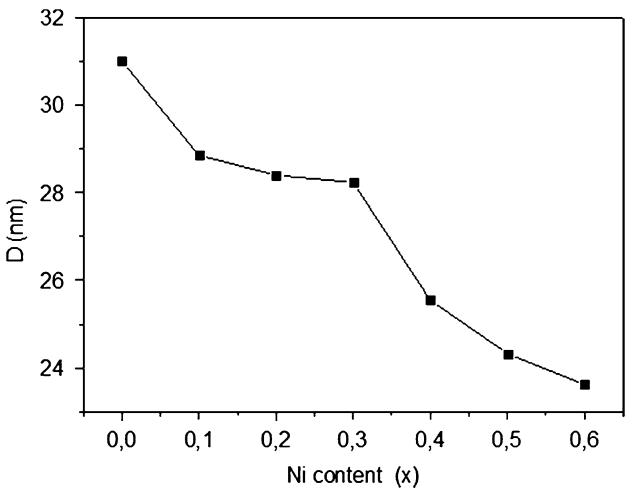


**Fig. 8** Crystallite size of $LaAl_{1-x}Ni_xO_{3-\delta}$ powders ($0 \leq x \leq 0.6$)

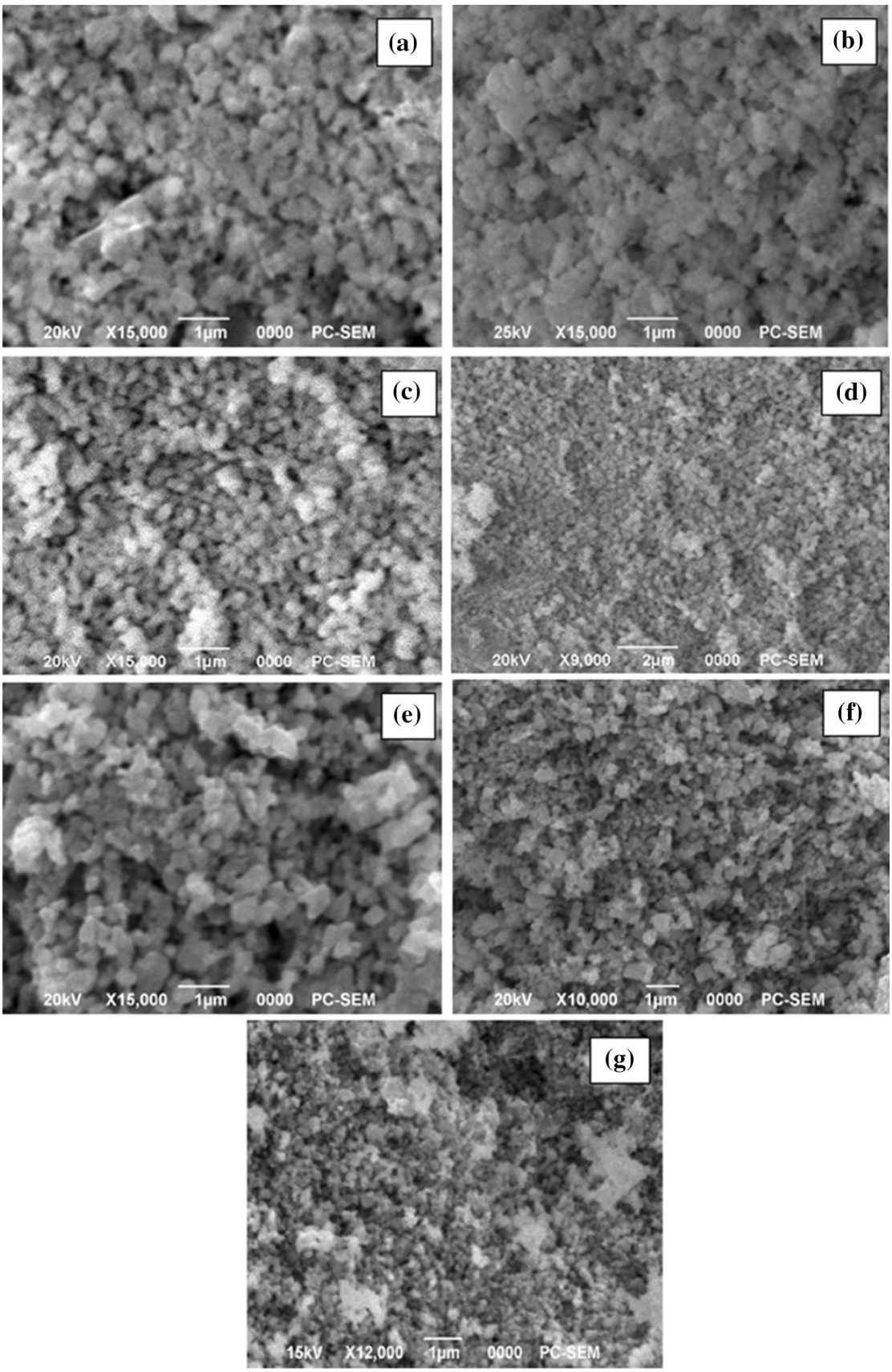
(a)
20kV X15,000 1μm 0000 PC-SEM
(b)
25kV X15,000 1μm 0000 PC-SEM
(c)
20kV X15,000 1μm 0000 PC-SEM
(d)
20kV X9,000 2μm 0000 PC-SEM
(e)
20kV X15,000 1μm 0000 PC-SEM
(f)
20kV X10,000 1μm 0000 PC-SEM
(g)
15kV X12,000 1μm 0000 PC-SEM

◀**Fig. 9** SEM micrographs of $LaAl_{1-x}Ni_xO_{3-}$: **a** $x = 0$, **b** $x = 0.1$, **c** $x = 0.2$, **d** $x = 0.3$, **e** $x = 0.4$, **f** $x = 0.5$ and **g** $x = 0.6$, calcined at 700 °C

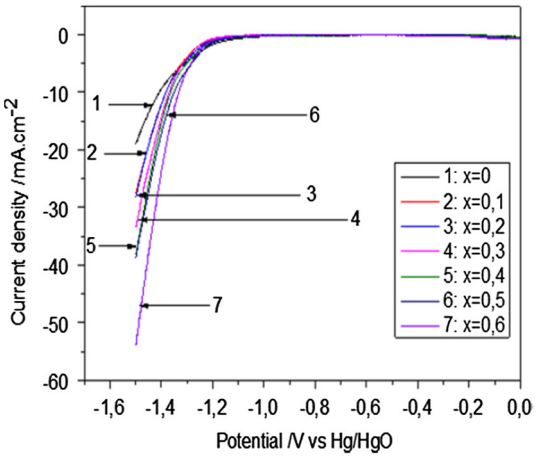


**Fig. 10** The *i–E* polarization curves of oxygen reduction for $LaAl_{1-x}Ni_xO_{3-\delta}$ electrodes in 1 M KOH

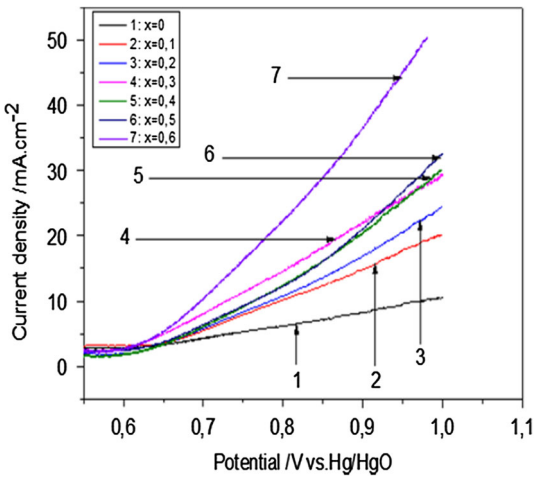


**Fig. 11** The *i–E* polarization curves of oxygen evolution for $LaAl_{1-x}Ni_xO_{3-\delta}$ electrodes in 1 M KOH

used in the preparation of the precipitate. The same result was also found for samarium-doped ceria powders [50] and $La_{1-x}Ca_xAlO_3$ oxides [51]. It has been shown that treating the precipitate with water and ethanol allows interactions between particles which leads during drying to the formation of chemical bonds.

### 3.5 Electrochemical Properties

The electrochemical activity for oxygen reduction and evolution reactions was investigated on $LaAl_{1-x}Ni_xO_{3-\delta}$ coated nickel substrate. The critical properties to consider when choosing an electrocatalyst support include its electrical conductivity surface area macromorphology microstructure corrosion resistance and cost [52]. The substrate of nickel satisfies these criteria and is often used in literature [53, 54]. Polarization studies under potentiostatic conditions were carried out. Figures 10 and 11 depict the cathodic and anodic current–potential curves of air electrode with different substitutions of nickel. The coated electrode films showed good adherence during polarization. The voltammetric profile is rather featureless, showing a wide plateau region see Figs. 10 and 11. It is clear that the coated perovskite electrodes present a wide range of electrochemical stability and a composition dependency of the current intensity. Electrode reactions over the surface of the oxides exhibit high currents. Compounds with large $x$ values show higher cathodic and anodic currents than those with smaller $x$. Compared to all compositions, the $LaAl_{0.4}Ni_{0.6}O_{3-\delta}$ one appears to be the most active. Nickel, a trivalent cation increases the catalytic activity and provides a catalyst with high structural stability due to the essential role of the transition metal ion in developing highly active catalysts. At the same voltage, the highest electrode performance is achieved for oxygen reduction and evolution with $x = 0.6$.

## 4 Conclusions

The co-precipitation method was successfully used for the synthesis of single phase for all $LaAl_{1-x}Ni_xO_{3-\delta}$ powders, employing nitrate salts of lanthanum, aluminium and nickel as cations precursors and mixture of sodium hydroxide such as base precipitant, at a relatively low temperature. The decomposition of the precursor hydroxides at 700 °C for 6 h, leads to the formation of phase pure perovskite with no detectable secondary phase as confirmed by XRD and FT-IR.

The microstructure and morphology of the compounds show that the samples particles are nearly spherical in shape and the powders are partially agglomerated. Compared to all studied compositions, $LaAl_{0.4}Ni_{0.6}O_{3-\delta}$ electrode exhibits significantly greater electroactivity, indicating that this material is among the analyzed series the best electrocatalyst for oxygen reduction and evolution.

## References

1. T. Ishihara, H. Matsuda, Y. Takita, J. Am. Chem. Soc. **116**, 3801 (1994)
2. J.W. Stevenson, T.R. Armstrong, D.E. McCready, L.R. Pederson, W.J. Weber, J. Electrochem. Soc. **144**, 3613 (1997)
3. P. Huang, A. Petric, J. Electrochem. Soc. **143**, 1644 (1996)

4. K.Q. Huang, R.S. Tichy, J.B. Goodenough, J. Am. Ceram. Soc. **81**, 2565 (1998)
5. K. Huang, M. Feng, J.B. Goodenough, J. Am. Ceram. Soc. **79**, 1100 (1996)
6. K. Huang, M. Feng, J.B. Goodenough, M. Schmerling, J. Electrochem. Soc. **143**, 3630 (1996)
7. T. Horita, K. Yamaji, N. Sakao, H. Yokokawa, A. Weber, E.-I. Tiffee, J. Electrochem. Soc. **148**, 456 (2001)
8. K.W. Browall, O. Muller, R.H. Doremus, Mater. Res. Bull. **11**, 1475 (1976)
9. C.B. Alcock, J.W. Fergus, L. Wang, Solid State Ionics **51**, 291 (1992)
10. T.L. Nguyen, M. Donkiya, S. Wang, H. Tagawa, T. Hashimoto, Solid State Ionics **130**, 229 (2000)
11. J. Mizusaki, I. Yasuda, J. Shimoyama, S. Yamauchi, K. Fueki, J. Electrochem. Soc. **140**, 67 (1993)
12. P.S. Anderson, G.C. Mather, F.M.B. Marques, D.C. Sinclair, A.R. West, J. Eur. Ceram. Soc. **19**, 1665 (1999)
13. P.S. Anderson, F.M.B. Marques, D.C. Sinclair, A.R. West, Solid State Ionics **118**, 229 (1999)
14. K. Nomura, S. Tanase, Solid State Ionics **98**, 229 (1997)
15. D. Lybye, F.W. Poulsen, M. Mogensen, Solid State Ionics **128**, 91 (2000)
16. J.A. Kilner, R.J. Brook, Solid State Ionics **6**, 237 (1982)
17. T. Takahashi, H. Iwahara, Energ. Convers. **11**, 105 (1971)
18. J.A. Kilner, P. Barrow, R.J. Brook, M.J. Norgett, J. Power Sources **3**, 67 (1978)
19. T. Ishihara, H. Matsuda, T. Takita, J. Electrochem. Soc. **141**, 3444 (1994)
20. B. Delmon, J. Droguest, in: W.H. Fuhn (Ed.), in *Proceedings of the 2nd International Conference on Fine Particles* (The Electrochemical Society, 1973), p. 242
21. R. Spinicci, P. Marini, S. Rossi, M. Faticanti, P. Porta, J. Mol. Catal. A: Chem. **176**, 253 (2001)
22. P. Ciambelli, S. Cimino, G. Lasorella, L. Lisi, S. De Rossi, M. Faticanti, G. Minelli, P. Porta, Appl. Catal., B: Environ. **37**, 231 (2002)
23. S. Cimino, L. Lisi, S. De Rossi, M. Faticanti, P. Porta, Appl. Catal., B : Environ. **43**, 397 (2003)
24. M. Parvary, S.H. Jazayeri, A. Taeb, C. Petit, A. Kiennemann, Catal. Commun. **2**, 357 (2001)
25. P. Moradi, M. Parvary, Iran. J Chem. Eng. **3**, 329 (2006)
26. H. Provendier, C. Petit, C. Estournès, S. Libs, A. Kiennemann, Appl. Catal. A **180**, 163 (1999)
27. M.A.C.G. van de Graaf, J.H.H. ter Matt, A.J. Burggraaf, J. Mater. Sci. **20**, 1407 (1985)
28. G. Silva, J. Santos, D. Martinelli, A. Pedrosa, M. de Souza, D. Melo, Mater. Sci. Appl. **1**, 39 (2010)
29. S.M. de Lima, J.M. Assaf, Mater. Res. **5**, 329 (2002)
30. Z.Q. Tian, W. Huang, Y. Liang, Ceram. Int. **10**, 1016 (2008)
31. S.K. Behera, P.K. Sahu, S.K. Pratihar, S. Bhattacharyya, Mater. Lett. **58**, 3710 (2004)
32. S. Bhattacharyya, S.K. Pratihar, R.K. Sinha, R.C. Behera, R.I. Ganguly, Mater. Lett. **53**, 425 (2002)
33. P.R.N. Silva, A.B. Soares, Ecl. Quím. São Paulo **34**, 31 (2009)
34. Chia-Liang Kuo, Yen-Hwei Chang, Moo-Chin Wang, Ceram. Int. **35**, 32 (2009)
35. L. Djoudi, M. Omari, N. Madoui, EPJ. Web. Conf. **29**, 00016 (2012)
36. H. Cui, M. Zayat, D. Levy, J. Non-Cryst. Solids. **352**, 3035 (2006)
37. D.S. Melo, É.P. Marinho, L.E.B. Soledade, D.M.A. Melo, S.J.G. Lima, E. Longo, I.M.G. Santos, A.G. Souza, J. Mater. Sci. **43**, 551 (2008)
38. A. Baranauskas, D. Jasaitis, A. Kareiva, Vibr. Spectrosc. **28**, 263 (2002)
39. J. Livage, M. Henry, C. Sanchez, Prog. Solid State Chem. **18**, 259 (1988)
40. C.J. Brinker, G.W. Scherrer, *Sol–Gel Science: The Physics and Chemistry of Sol–Gel Processing* (Academic Press, Inc, New York, 1990), pp. 59–64
41. B. Schrader (ed.), *Infrared Raman Spectroscopy: Methods and Applications* (VCH, Weinheim, 1995)
42. T. Vaz, A.V. Salker, Mater. Sci. Eng., B **143**, 81 (2007)
43. R.D. Shannon, Acta Crystallogr. Sect. A **32**, 751 (1976)
44. G. Valderrama, A. Kiennemann, M.R. Goldwasser, Catal. Today **133–135**, 142 (2008)
45. D. Zhou, G. Huang, X. Chen, J. Xu, S. Gong, Mater. Chem. Phys. **84**, 33 (2004)
46. C.L. Kuo, C.L. Wang, T.Y. Chen, G.J. Chen, I.M. Hung, C.J. Shih, K.Z. Fung, J. Alloys Compd. **440**, 367 (2007)
47. S. Sompech, A. Srion, A. Nuntiya, Science Asia **38**, 102 (2012)
48. J. Tulloch, S.W. Donne, J. of Power Sources **188**, 359 (2009)
49. N. Mota, M.C. Alvarez-Galvána, R.M. Navarroa, J.L.G. Fierroa, S.M. Al-Zahranib, A. Goguetc, H. Dalyc, W. Zhangd, A. Trunschked, R. Schlögld, Appl. Catal B: Environ. **113**, 271 (2012)
50. G.B. Jung, T.J. Huang, M.H. Huang, C.L. Chang, J. Mater. Sci. **36**, 5839 (2001)
51. M. Diafi, M. Omari, Bol. Soc. Esp. Ceram. Vidr. **51**(6), 337 (2012)
52. W. Li, X. Wang, Z. Chen, M. Waje, Y. Yan, J. Phys. Chem. B **110**, 15353 (2006)
53. R.N. Singh, A. Singh, D. Mishra, Anindita, P. Chartier, J. Power Sources **185**, 776 (2008)
54. B. Lal, M.K. Raghunandan, M. Gupta, R.N. Singh, Int. J. Hydrogen Energy **30**, 723 (2005)